Structure and Interfacial Aspects of Self-Assembled Cationic Lipid−DNA Gene Carrier Complexes§

Joachim O. Rädler,*,† Ilya Koltover, Amanda Jamieson, Tim Salditt,‡ and Cyrus R. Safinya*

Materials Department, Physics Department, and Biochemistry and Molecular Biology Program, University of California, Santa Barbara, California 93106

Received March 31, 1998

Cationic lipid−DNA (CL−DNA) complexes were recently found to exhibit a novel multilamellar structure composed of alternating lipid bilayer and DNA monolayer with distinct interhelical DNA spacings (Rädler et al. *Science* **1997**, *275*, 810). We report on the aggregation behavior, morphology, and interfacial properties related to the solution structure of DOPC/DOTAP−DNA complexes. Using optical microscopy and synchrotron X-ray diffraction, we found two discrete regimes for the complex size and surface charge as a function of the lipid-to-DNA mass ratio. The regimes correspond to the coexistence of complexes with either excess DNA or excess liposomes, characterized by a negative and positive surface potential of the complexes, respectively. The internal structure in these cases exhibited different but constant DNA packing distances of 35 and 46 Å, respectively. The regimes are separated by a transition region around the isoelectric point, where the number of cationic lipids equals the number of DNA phosphate groups. At the isoelectric point the average complex size diverged and the DNA packing spacing is described by a simple volume fraction calculation. The complex formation occurred on three time scales: rapid condensation, a slower colloidal aggregation, and finally, a long term reorganization or compaction. Complexes with positive surface charge were shown to adhere to negatively charged giant liposomes.

Introduction

The transfer of extracellular genetic material into different types of eucaryotic cells is the goal of gene therapy. One strategy is to construct synthetic, virus-like vectors, which are composed of recombinant plasmid DNA complexed with cationic reagents. Felgner et al. found in 1987 that the uptake of exogenous DNA by eucaryotic cells is considerably facilitated, if the anionic polynucleic acid is previously complexed with cationic liposomes.[1] The protocol known as "lipofection" results in transient or stable expression of a foreign gene and is widely used in molecular biology.[2−6] Experiments have also demonstrated the feasibility of transfection in vivo.[7] Over the last 10 years it has been found that transfection is mediated by a wide class of cationic lipids and cationic polymers, yielding higher or comparable transfection efficiency than previously established synthetic nonviral gene delivery methods including CaP precipitation or DEAE dextran complexation.[5,8−10] However, synthetic delivery systems are still vastly inefficient compared to viral transduction. This is partly due to our lack of knowledge regarding the path of entry and the barriers and enzymatic attacks encountered upon entry into targeted cells. The following, highly qualitative picture, which needs further experimental confirmation, has emerged: the DNA complexes enter the cell by endocytosis, subsequently fuse with or lyse the endosomal membrane and release the DNA into the cytoplasm.[11−14] Little is known about how DNA reaches the nucleus. This step may be forced by mass action, i.e., by the input of a large excess amount of plasmid DNA.[12]

Surprisingly little attention has been given to the internal structure of DNA−lipid complexes and the interfacial properties of CL−DNA complexes. In the original work by Felgner et al. it was proposed that cationic liposomes were attached to the DNA strand like beads on a string. Electron microscopy (EM) studies have been reported on string-like structures and indications of fusion of liposomes in metal-shadowing EM,[15] and tube-like images possibly depicting lipid bilayer-covered DNA were observed in freeze-fracture EM.[16] In particular, oligolamellar structures had been reported previously in cryo-TEM studies.[17,18] DNA and cationic liposomes in fact

* To whom correspondence should be addressed.

† Present address: Physikdepartment, Technische Universität München, Institut für Biophysik (E22), James Franck-Strasse 1, 85747 Garching, Germany.

‡ Present address: Sektion Physik, Ludwig Maximilian Universität München, Germany.

§ Abbreviations: DOPC (dioleoylphosphatidylcholin), DOPE (dioleoylphosphatidylethanolamine), DOTAP (dioleoyltrimethylammoniopropane), *λ*-DNA (DNA from *λ*-phage).

(1) Felgner, P. L.; Gadek, T. R.; Holm, M.; Roman, R.; Chan, H. W.; Wenz, M.; Northrop, J. P.; Ringold, G. M.; Danielson, M. *Proc. Natl. Acad. Sci. U.S.A.* **1987**, *84*, 7413.

(2) Hug, P.; Sleight, R. G. *Biochim. Biophys. Acta* **1991**, *1097*, 1−17.

(3) Behr, J.-P. *Bioconjugate Chem.* **1994**, *5*, 382−389.

(4) Rose, J. K.; Whitt, B.; Whitt, M. A. *BioTechniques* **1991**, *10*, 520−525.

(5) Remy, J.-S.; Sirlin, C.; Vierling, P.; Behr, J.-P. *Bioconjugate Chem.* **1994**, *5*, 647−654.

(6) Budker, V.; Gurevich, V.; Hagstrom, J. E.; Bortzov, F.; Wolff, J. A. *Nature Biotechnol.* **1996**, *14*, 760−764.

(7) Zhu, N.; Liggitt, D.; Liu, Y.; Debs, R. *Science* **1993**, *261*, 209−211.

(8) Pinnaduwage, P.; Schmitt, L.; Huang, L. *Biochim. Biophys. Acta* **1989**, *985*, 33−37.

(9) Felgner, J. H.; Kumar, R.; Sridhar, C. N.; Wheeler, C. J.; Tsai, Y. J.; Border, R.; Ramsey, P.; Martin, M.; Felgner, P. L. *J. Biol. Chem.* **1994**, *269*, 2550−2561.

(10) Legendre, J.-Y.; Szoka, F. C., Jr. *Proc. Natl. Acad. Sci. U.S.A.* **1993**, *90*, 893−897.

(11) Wrobel, I.; Collins, D. *Biochim. Biophys. Acta* **1995**, *1235*, 296−304.

(12) Zabner, J.; Fasbender, A. J.; Moninger, T.; Poellinger, K. A.; Welsh, M. J. *J. Biol. Chem.* **1995**, *270*, 18997−19007.

(13) Hui, S. W.; Langer, M.; Zhao, Y.-L.; Ross, P.; Hurley, E.; Chan, K. *Biophys. J.* **1996**, *71*, 590−599.

(14) Xu, Y.; Szoka, F. C. J. *Biochemistry* **1996**, *35*, 5616−5623.

(15) Gershon, H.; Ghirlando, R.; S. B., G.; Minsky, A. *Biochemistry* **1993**, *32*, 7143−7151.

(16) Sternberg, B.; Sorgi, F. L.; Huang, L. *FEBS Lett.* **1994**, *356*, 361−366.

S0743-7463(98)00360-6 CCC: $15.00
Published on Web 06/26/1998

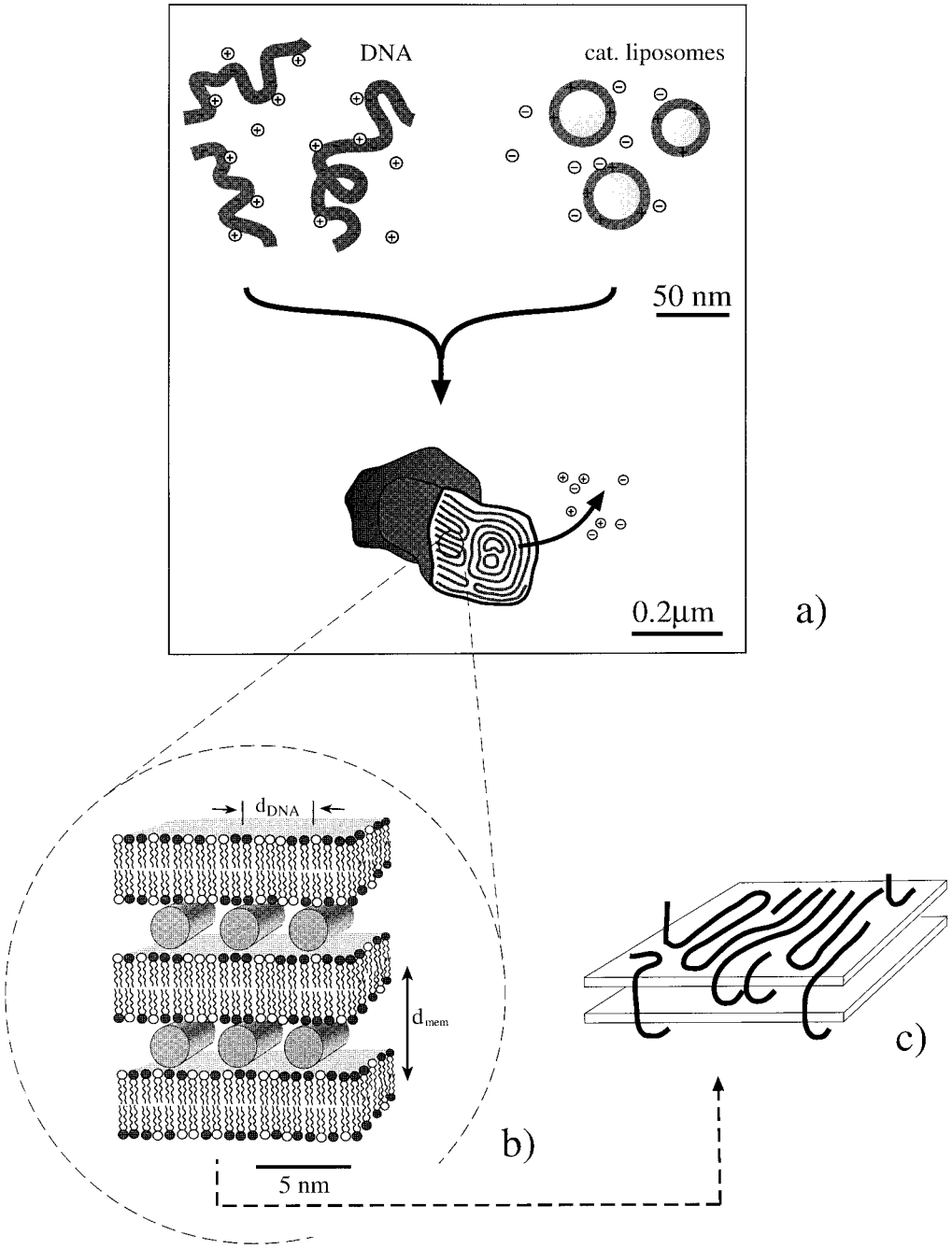

Figure 1. (a) Schematic drawing of the collapse of DNA and cationic liposomes into dense multilamellar aggregates. The condensation is driven by the release of bound counterions. (b) The local structure of the self-assembled DNA−lipid complexes is characterized by a defined membrane repeat distance, d_{mem}, and a 2-dimensional in-plane packing of the DNA strands with interhelical spacing d_{DNA}. The semiflexible DNA double-helices are represented by rods, and the lipid headgroups of the neutral and cationic lipids are shown in light and dark shade. (c) Closeup of the in-plane arrangement of the DNA strands. Defects will limit the 2-dimensional smectic order to finite size domains.

undergo a radical topological transition whereby the liposomes rupture and fuse into condensed multilamellar structures. We recently investigated the cationic lipid mixture DOPC/DOTAP complexed with λ-phage DNA using high-resolution synchrotron X-ray diffraction. The DNA−cationic lipid complexes formed multilamellar liquid crystalline aggregates with two-dimensional in-plane order of DNA intercalated between the lipid membranes.[19,20] A schematic drawing of the condensation process and the local structure on different scales is shown in Figure 1.

In this article we show that interfacial properties such as the aggregation behavior and the overall morphology of the complexes are related to the local liquid crystalline structure. Optical microscopy studies on mixtures of sonicated DOPC/DOTAP liposomes and λ-phage DNA reveal the aggregation of DNA and lipid into optically birefringent globules. These complexes coexist with excess

(17) Gustafsson, J.; Arvidson, G.; Karlsson, G.; Almgren, M. *Biochim. Biophys. Acta* **1995**, *1235*, 305−312.
(18) Lasic, D. D.; Strey, H.; Stuart, M. C. A.; Podgornik, R.; Frederik, P. M. *J. Am. Chem. Soc.* **1997**, *119*, 832−833.
(19) Rädler, J. O.; Koltover, I.; Salditt, T.; Safinya, C. R. *Science* **1997**, *275*, 810−814.
(20) Salditt, T.; Koltover, I.; Rädler, J. O.; Safinya, C. *Phys. Rev. Lett.* **1997**, *79*, 2582−2585.

liposomes or excess DNA unless the stoichiometric charge neutral composition is met. In the coexistence regime, the aggregates exhibit a constant structure with a DNA-packing distance $d_{DNA} = 35$ Å for complexes coexisting with liposomes and $d_{DNA} = 46$ Å for complexes coexisting with DNA. The former were shown to be positively charged, while the latter complexes were negatively charged. The two regimes are separated by the isoelectric transition regime, which is macroscopically characterized by a pronounced increase in the size of the CL−DNA aggregates. Most notably, the structure in the charge neutral regime was found to be a well-defined intercalated array of DNA between cationic membranes. The DNA repeat spacing in this case is quantitatively described by a simple equation based on a volume fraction calculation. Giant DMPC/DMPG (9:1) liposomes were used to simulate the adhesion properties of complexes to cell surfaces. Positevely charged CL−DNA complexes with a lipid-to-DNA ratio of L/D > 5 readily adhere to giant liposomes and were even found to be internalized after heat cycling over the chain-melting temperature. The liquid crystalline textures of CL−DNA aggregates at high concentration were investigated using crossed polarizers. The aggregates were found to be composed of a network of globules with smectic textures, which in some cases exhibited twisted superstructures on a several micrometer scale.

Materials and Methods

DNA, Liposome, and Complex Preparation. All lipids, DOPC (dioleoylphosphatidylcholin), DOPE (dioleoylphosphatidylethanolamine), and DOTAP (dioleoyltrimethylammoniopropane) were purchased from Avanti Polar Lipids. The chemical structure formulas are given in Figure 2. Cationic liposomes were prepared as follows. A mixture of DOPE/DOTAP and DOPC/DOTAP with given mole ratios respectively were dissolved in chloroform at 20 mg/mL. A 500 mL aliquot of the stock solution was dried under nitrogen in a 25 mL glass beaker and desiccated under vacuum for 6 h. After addition of 2.5 mL of Millipore water and 2 h incubation at 40 °C, the vesicle suspension was sonicated to clarity for 10 min. The resulting liposome solution (25 mg/mL) was filtered through 0.2 μm Nucleopore filters. Purified λ-phage DNA was purchased from New England Biolabs (Beverly, MA) and X-ray data were taken with linear λ-DNA prepared in 2 ways: (1) used as delivered and (2) linearized by heating to 65 °C, reacted with a surplus of a 12-base oligo complementary to the 3′ COS end, and subsequently ligated (T4 DNA ligase, Fischer). The methods gave the same X-ray scattering results.

Optical Techniques. Optical observations were carried out using a Nikon Diaphot 300 equipped for epifluorescence and high-resolution DIC (60×, 1.4 N.A. objective, fiber illumination). Images were taken with a high-resolution tube camera (VE 1000, Dage-MTI Inc., Michigan City, IN), and video enhancement processing was carried on a DSP 2000 (Dage-MTI). The video signal was digitized by a Scion LG-3 frame grabber card using NIH image software. For fluorescence microscopy, liposomes were prepared with 0.2 mol % DHPE-Texas Red (Molecular Probes) fluorescence label. DNA was labeled using the intercalating dye YOYO (Molecular Probes) at a dye to base pair ratio 1:10. Fluorescence images were taken with a SIT camera (VE 1000 SIT, Dage-MTI). DNA−cationic lipid complexes were prepared by mixing the DNA solution (0.1 mg/mL) and liposome solution (0.5 mg/mL). To avoid inhomogeneities, the concentration of the stock solutions was adjusted such that almost equal volumes were mixed each time. Typically, the samples were investigated 30 min after mixing. The hydrodynamic radius of the liposomes and of the DNA−lipid complexes was measured using a commercial dynamic light scattering setup (Microtrac UPA 150, Leeds and Northrup). The surface potential of the DNA−lipid complexes was determined from their electrophoretic mobility using the ZetaPlus potentiometer (Microtrac, Brookhaven Instruments).

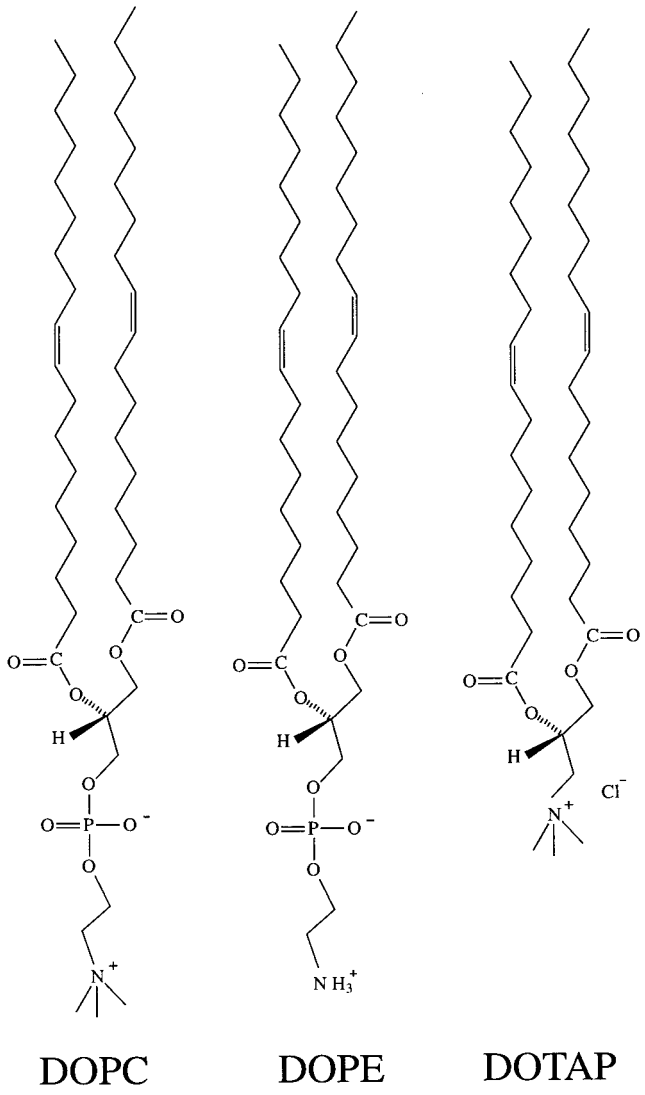

Figure 2. Chemical structure formula of DOPC (dioleoylphosphatidylcholin), DOPE (dioleoylphosphatidylethanolamine), and DOTAP (dioleoyltrimethylammoniopropane).

Digestion Assays. DNA−cationic lipid complexes were tested against restriction enzymes in order to assay the degree of protection provided by the complex structure. DNA−lipid complexes were prepared as above for different lipid-to-DNA ratios in Millipore water. After 15 min the buffer conditions were adjusted by a 10× reaction buffer (Tris, pH 6.8, Mg). Then Hind III enzyme was added and incubated for 3 h at 37 °C. The reaction was stopped by phenol (1:1 by volume). Subsequently, the lipid was removed by adding 1% SDS and chloroform extraction. The remaining DNA fragments were separated by gel electrophoresis (1% agarose).

X-ray Diffraction. High-resolution synchrotron X-ray scattering experiments were performed at the Stanford Synchrotron Radiation Laboratory on beam-line 7-2. X-ray radiation at 8 keV was selected, and the resolution was set by vertical and horizontal slits before and after the sample. The longitudinal resolution (HWHM) was 0.0003 Å^{-1}. Lower resolution X-ray scattering experiments were performed in house at the UCSB's Materials Research Laboratory X-ray facility equipped with a 18 kW rotating anode (Rigaku-RU300). A bent (002) graphite crystal was used to focus the beam. Scans were taken in a $\theta-2\theta$ mode using a scintilator (Bicron) detector. The intensities are presented as a function of the scattering wave vector $q = 4\pi/\lambda \sin\theta$, with scattering angle 2θ and X-ray wavelength $\lambda = 1.54$ Å. The position and the full width half-maximum (fwhm) values of the observed Bragg diffraction peaks were determined by fitting to Lorentzian line shapes.

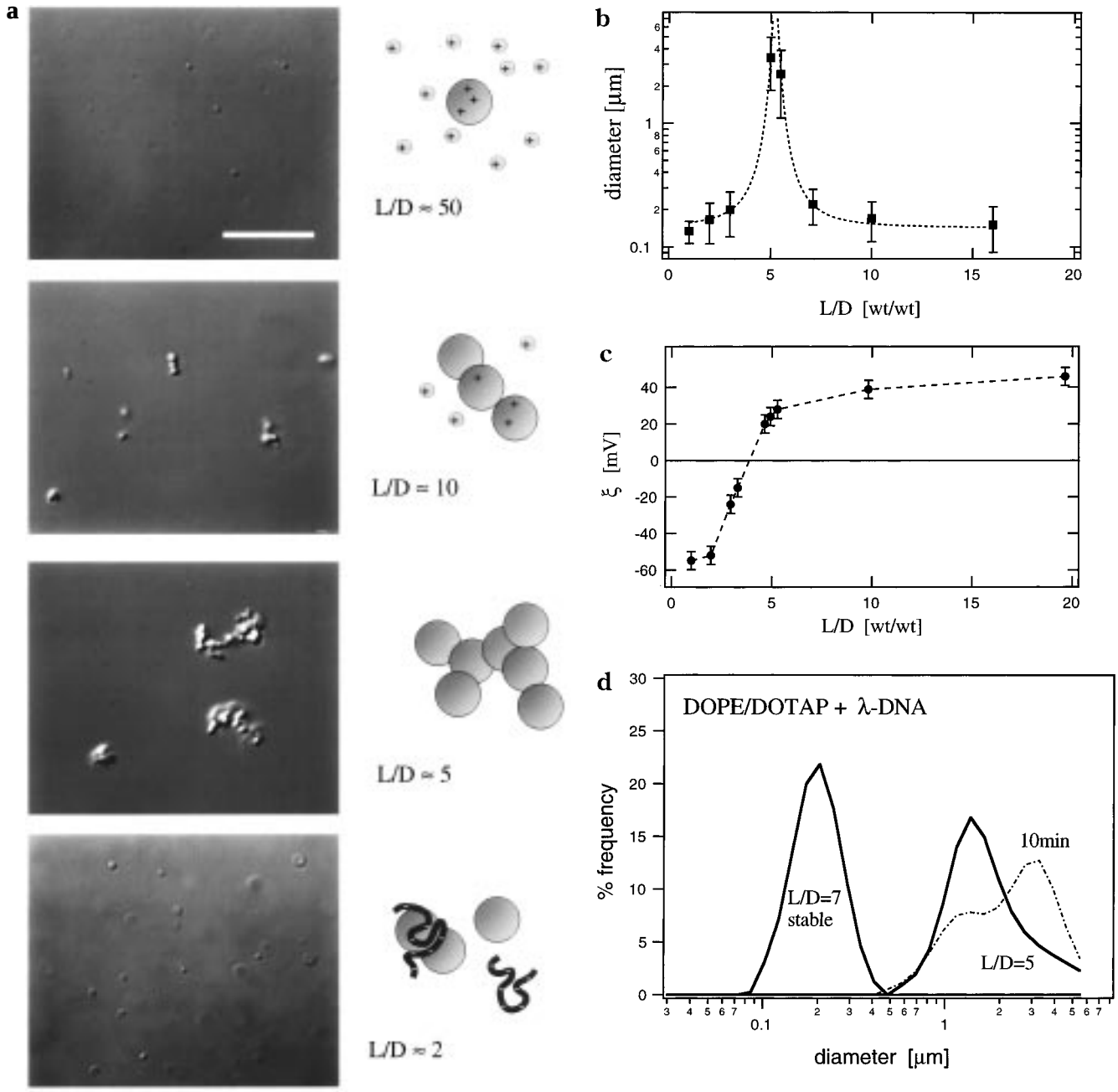

Figure 3. (a) High-resolution DIC images of DNA−lipid complexes (forming distinct condensed globules) observed 30 min after mixing (λ-DNA with sonicated DOPE/DOTAP (1:1) liposomes (0.1 mg/mL)). In mixtures of different lipid to DNA mass ratios (L/D) the following complexes are found: L/D = 50, small and positively charged isolated globules; L/D = 10, strings of positively charged aggregated globules; L/D = 5, flocculation of DNA−lipid globules due to charge neutrality; L/D = 2, small and negatively charged isolated globules. (b) Average size of the lipid−DNA complexes as a function of the lipid-to DNA ratio L/D measured by dynamic light scattering. (c) The ζ potential of the complexes shows sign reversal at about the stoichiometric L/D ratio for charge neutrality. (d) Examples of the size distribution as measured by dynamic light scattering. At a lipid-to-DNA ratio of L/D = 7 a stable distribution is obtained. In contrast, for L/D = 5 an evolution of the distribution with time (10 min, 20 min) is observed.

X-ray samples were prepared at higher concentrations than for the optical studies in order to improve on the signal-to-background intensity ratio (25 mg/mL liposomes and 5 mg/mL DNA). The local molecular order of the DNA aggregates is not concentration dependent.[19] Lipid and DNA solutions were directly filled into 2 mm diameter quartz capillaries, flame sealed, and centrifuged at low speed. Concentrated samples needed several days to equilibrate, after which period of time no change in the X-ray pattern was seen any more.

Results

Aggregation and Morphology. Measured by dynamic light scattering, the size distribution of sonicated and, furthermore, 0.2 μm filtered DOPC/DOTAP liposomes was found to peak around 700 Å. These liposomes were hardly resolvable using video-enhanced differential interference contrast (DIC) microscopy but yet visible as a diffuse background of rapidly moving particles. However, mixtures of λ-DNA and cationic liposomes revealed compact globules of higher contrast and considerably larger diameters than pure liposomes (Figure 3a). The optically dense globules appeared birefringent under crossed polarizers. The size distribution of these CL−DNA globules depended strongly on the lipid-to-DNA mass ratio (L/D). In mixtures that contained small amounts of DNA, globules formed that coexisted with excess liposomes. With increasing DNA content more and larger

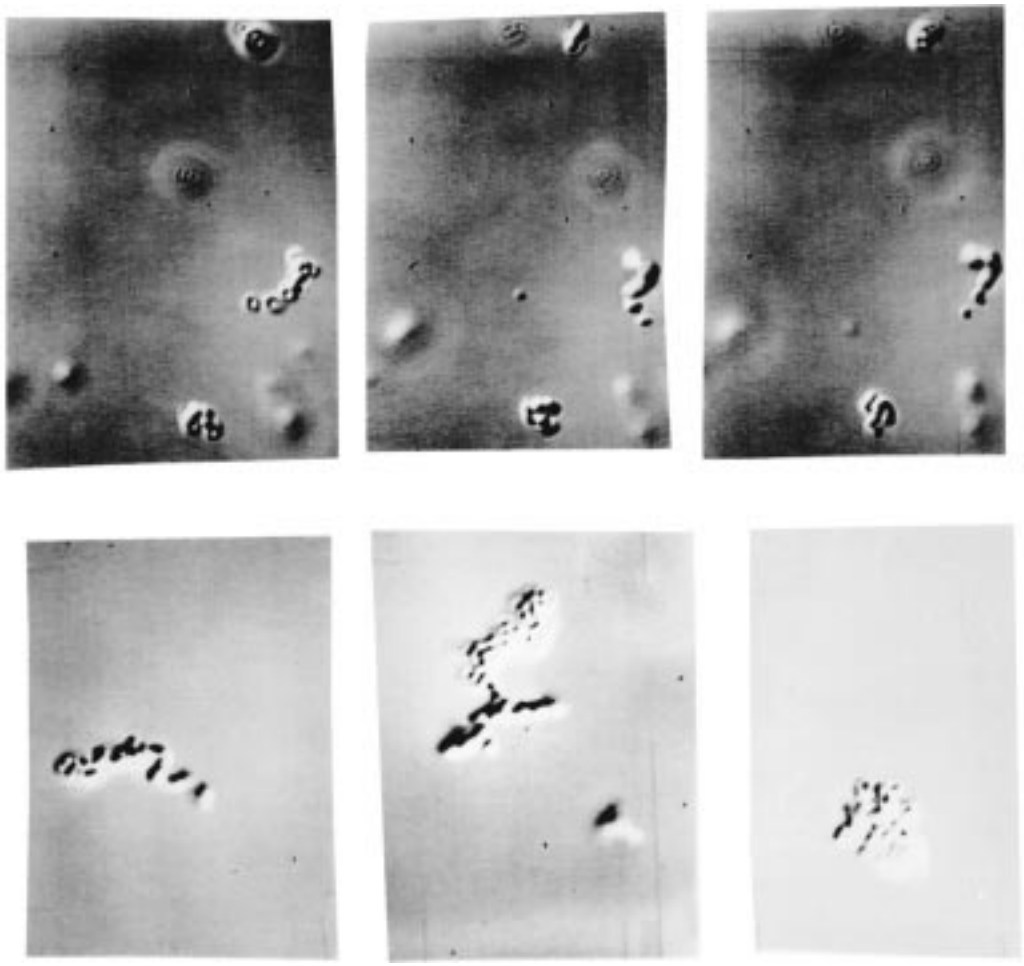

Figure 4. (a) Optical micrographs showing the time-dependent aggregation and compaction of DNA−lipid complexes in the charge neutral (L/D = 5) regime.

aggregates formed. The larger aggregates appeared to be made of distinct globular units of remarkably constant size. Around the lipid-to-DNA mass ratio L/D = 5 the aggregates precipitated into huge (>10 μm) flocculates. The time scale of flocculation is concentration dependent and lasted several hours in dilute solutions. Mixtures of liposomes and DNA with L/D < 4 formed again small aggregates that were stable over time.

We measured the size distribution of DNA−lipid aggregates independently by dynamic light scattering. The average size of the DNA−lipid globules as a function of L/D was found to be in good agreement with the microscopic observations. The size clearly diverged around L/D = 5 close to the point of charge neutrality L/D = 4.4 (see Figure 3b). The large error bars indicate the broad polydispersity of the system. The ζ potential of the globules was determined from their electrophoretic mobility in an external electric field. The surface potential of globules at large L/D was found to be +40 mV. In the other extreme case (L/D $\ll$ 5), an excess amount of DNA led to globules of about −60 mV. The ζ potential reversed sign at exactly the stoichiometric neutral charge lipid-to-DNA ratio (Figure 3c).

The CL−DNA complexes are composed of lipid and DNA at an almost stoichiometric charge neutral ratio. However, in the presence of excess liposomes the complexes exhibit a positive surface potential. In the presence of excess DNA negatively charged complexes are formed. Interestingly, the change in the surface potential is accompanied by structural changes inside the complexes. As shown later in Figure 8b the DNA−DNA spacing in the negatively charged complexes is smaller than in positively charged ones. This may indicate that additional cationic lipid and DNA molecules are incorporated within, respectively, positive and negative complexes. As depicted schematically in Figure 3a, the size distribution and stability of the DNA−lipid aggregates can be understood in terms of a charge stabilized colloidal suspension. As described by the well-known DLVO theory, the competition of repulsive electrostatic and attractive van der Waals forces determines if a colloidal suspension is stable or tends to precipitate. Figure 3d shows the size distribution of the complexes as measured by dynamic light scattering for L/D = 7 and L/D = 5. While the positive complexes exhibited a narrow distribution, the almost charge neutral complexes are clearly larger and evolve over a time scale of several minutes to even larger structures.

The kinetics of the complex formation involves three time scales: A rapid liposome−DNA *condensation* yielding globular complexes and a slower colloidal *aggregation* of globules that is strongly dependent on the surface charge of the globules. On an even longer time scale the diffusion-aggregated complexes undergo a reorganization or *compaction*. The compaction is illustrated in Figure 4a. After more than 24 h the aggregates lost their fractal-like structure made of individual globular units and exhibit compact forms instead.

The cocondensation of DNA and lipid can be demonstrated by fluorescence microscopy. We fluorescently labeled DNA with YOYO-1 (λ_e = 509 nm) (Molecular Probes) and mixed TexasRed (λ_e = 633 nm) labeled lipid with the cationic lipid (0.2%). Figure 5a shows micro-

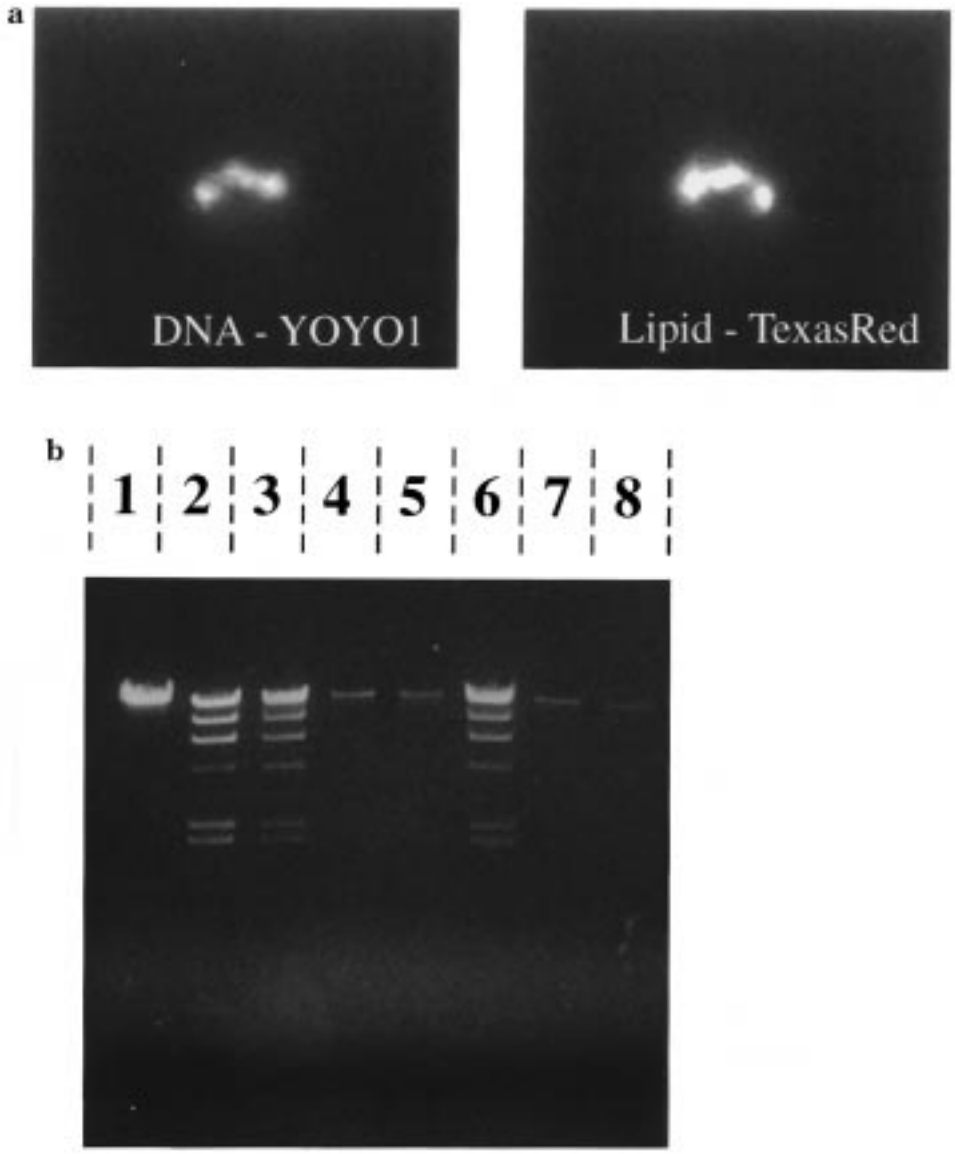

Figure 5. (a) Fluorescence micrographs of a CL−DNA complex showing the distribution of DNA (left) and lipid (right). (b) Electrophoresis bands of the digestion assay of DNA−cationic lipid complexes. The first two lanes show the control of undigested and fully Hind III digested λ-DNA. Lanes 3−5 show DNA previously complexed with DOPC/DOTAP (1:1) at a lipid-to-DNA ratio of L/D = 2, L/D = 5, and L/D = 10, respectively. Lanes 6−8 show DNA complexed with DOPE/DOTAP (1:1) at L/D = 2, L/D = 5, and L/D = 10, respectively. Complexes with large L/D > 5 were protected from the Hind III restriction enzyme.

graphs of fluorescence emission of condensed DNA−lipid globules at 633 and 509 nm, respectively. All complexes exhibited lipid and DNA fluorescence at the same time. The intensities of the globules are evenly distributed and exceed the fluorescence intensity of a single liposome and a single DNA molecule, respectively. These observations are consistent with a condensed lipid/DNA structure. The existence of chained globules also raises the question to which extent the cationic lipid covers the DNA strands and whether full or partial protection against enzymatic digestion is provided. We therefore performed DNA digestion experiments in order to assess the degree of accessibility of DNA in the lipid-complexed form. DOPC/DOTAP (1:1)−λ-DNA complexes with lipid-to-DNA ratios of L/D = 2, L/D = 5, and L/D = 15 were subjected to Hind III restriction enzyme. After removal of the enzyme and analysis of the DNA fragments by gel electrophoresis, different degrees of DNA degradation were revealed (Figure 5b). While naked DNA is clearly cut seven times into a classical Hind III ladder, DNA complexed with cationic lipid is fully protected for L/D = 5 and L/D = 15. Partial degradation is observed for L/D = 2, indicating that below the point of charge neutrality the excess DNA is not covered with lipid.

The adhesion properties of CL−DNA complexes were investigated using negatively charged giant liposomes as model surfaces. Figure 6a depicts DMPC/DMPG (9:1) liposomes imaged in Normaski contrast. Smooth multi- and unilamellar vesicles were found. In contrast, after addition of 2 μm sized DOPC/DOTAP (1:1) complexes, decorated liposomes were observed (Figure 6b). The fluorescence micrograph (Figure 6c) corresponding to the DIC image shown in Figure 6b proves that the liposomes were covered by DNA−lipid complexes. We carried out a series of adhesion experiments by testing the adhesion of the DNA/cationic lipid complexes as a function of L/D. Complexes with L/D < 4.4 did not stick to DMPC/DMPG liposomes, while complexes formed at L/D > 4.4 did, in agreement with the charge reversal of the complexes shown in Figure 3c. Most interestingly, we found that, if the system was cooled below the chain-melting temperature of DMPC/DMPG (9:1) and heated again, some

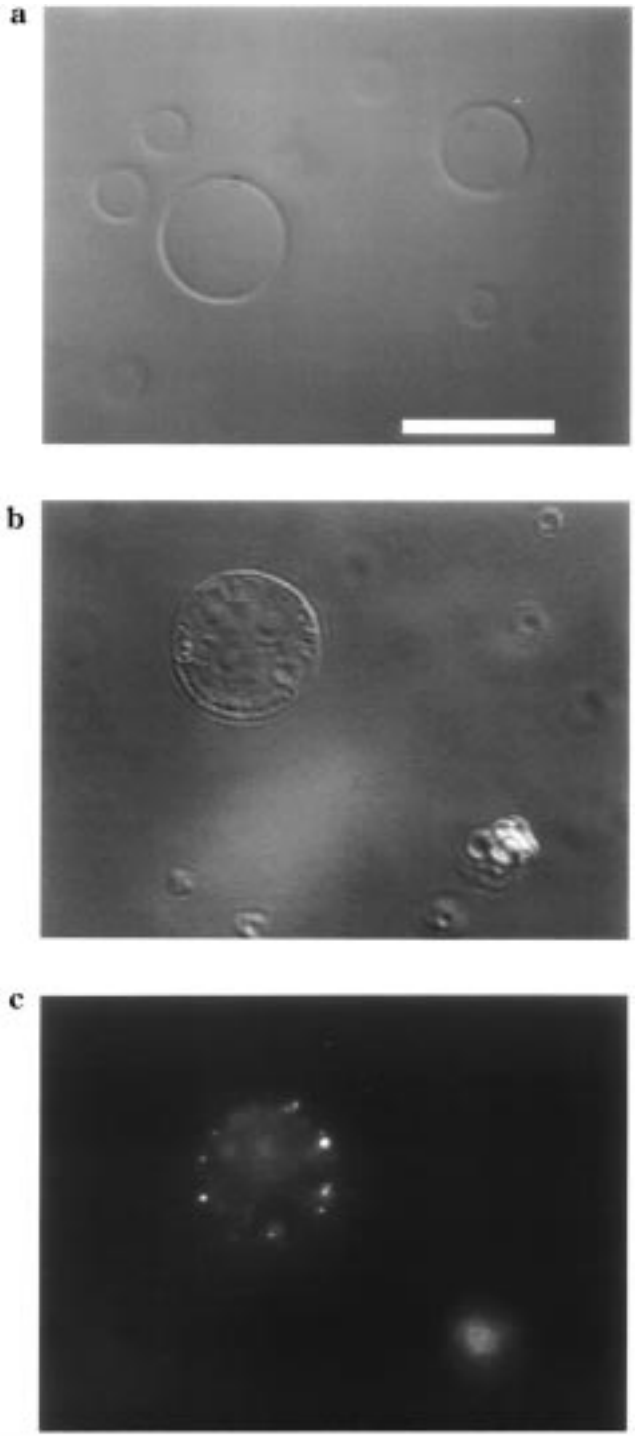

Figure 6. (a) Giant anionic DMPC/DMPG (9:1) liposomes (bilayer in the lipid chain frozen state). (b) Adhesion of DNA−cationic lipid complexes to the anionic liposome. (DIC) The giant liposomes appear decorated. (c) Fluorescence image of (b) showing the fluorescent-labeled DNA molecules.

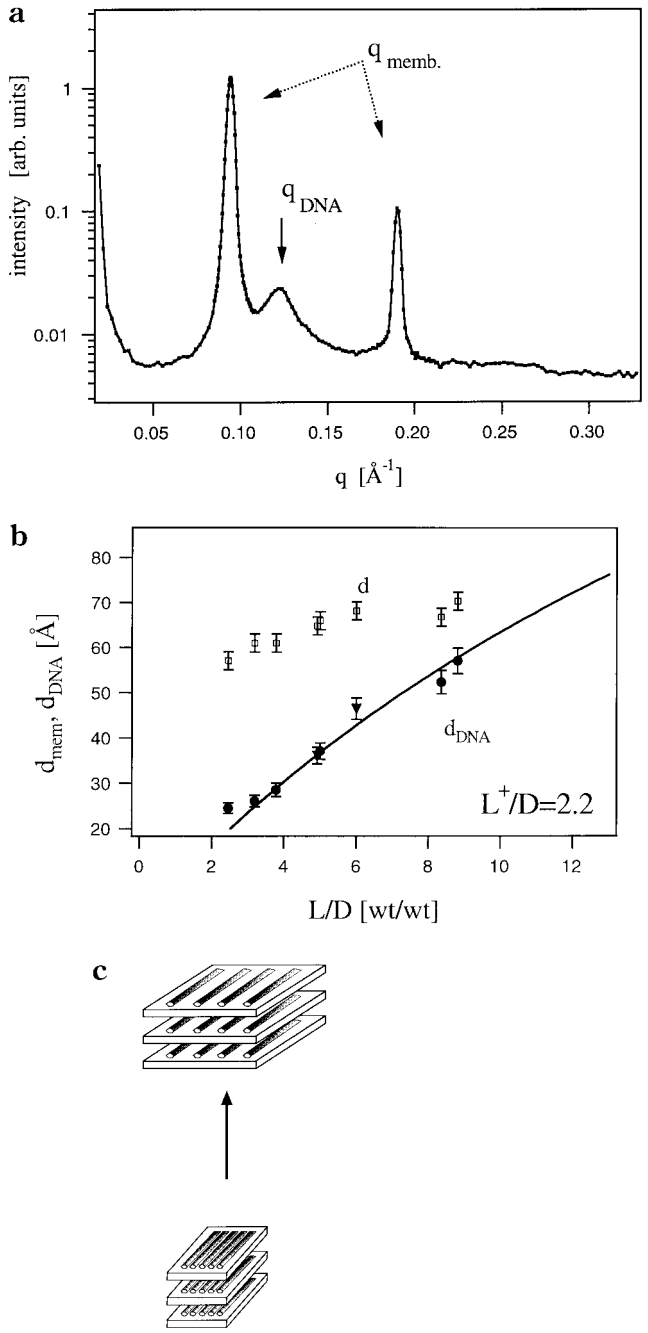

Figure 7. (a) Synchrotron small-angle X-ray scattering (SAXS) of DOPC/DOTAP−λ-DNA complexes at the isoelectric point as a function of the lipid-to-DNA mass ratio. The first sharp Bragg reflection and its second higher harmonic arise from lamellar membrane stacking. The additional broader peak (arrow) can be attributed to DNA−DNA in-plane correlation. The DNA correlation peak moves toward smaller q as more lipid is added. (b) Repeat distances plotted as a function of L/D. The one-dimensional DNA lattice with repeat distance d_{DNA} expands from 24.5 to 57.1 Å. The solid line is the prediction based on a constant volume fraction calculation (eq 4). (c) Schematic drawing of the expansion of the local structure as a function of the lipid-to-DNA ratio.

DNA fluorescent aggregates moved freely inside the decorated giant liposomes. In the immediate vicinity of the chain-freezing transition, one expects cracks and pore-like openings to form in the bilayer due to thermal contractions and expansions. Because the complexes are localized near the bilayer, some of them are able to travel through the openings into the vesicle interior, as observed experimentally.

X-ray Diffraction Studies. High-resolution X-ray diffraction was performed in order to elucidate the internal molecular structure of lipid−DNA aggregates. Figure 7a shows the scattering intensity of an isoelectric DOPC/DOTAP/λ-DNA mixture. Typically, strong, equally spaced Bragg reflections are observed with $q(001) = 0.097$ Å^{-1}. These reflections correspond to a multilamellar packing of the lipid membranes induced by the intercalation of a monomolecular layer of DNA. In addition, a broad

reflection is observed, which changes in shape and position as a function of lipid composition and lipid-to-DNA mass ratio and can be attributed to DNA−DNA in-plane packing. A schematic drawing (Figure 1) illustrates the proposed molecular structure of the lipid−DNA complexes.[19] The DNA molecules are intercalated between planar stacks of lipid bilayers and form a one-dimensional rod lattice.

The measured repeat distance $d = 65$ Å for the lamellar lipid−DNA stack is in agreement with an aqueous spacing of about 25 Å and a membrane thickness of $\delta_m = 40$ Å. This membrane spacing is in fact wide enough to accommodate DNA strands of 20 Å in diameter. Interestingly, the repeat distance of 65 Å is very close to the repeat distance of pure DOPC in water. This indicates that the intercalated DNA neutralizes the cationic lipid. In fact, without DNA the DOPC/DOTAP lipid−water phase forms vesicles in dilute solutions and lamellar phases in concentrated solutions, whereby the interlayer spacing is set by the water content. In the latter case the membrane thickness can be determined from the lamellar repeat distance, if the water content is known.[21] We used this method to determined independently the thickness of the binary DOPC/DOTAP membranes. We obtained $\delta_m = 39 \pm 0.3$ Å for a 1:1 mixture of DOPC/DOTAP, 37.2 ± 0.3 Å for pure DOTAP, and 42 ± 0.3 Å for pure DOPC. The difference in the bilayer thickness of pure DOTAP and pure DOPC must be attributed to the different headgroup volumes, since the dioleoyl hydrocarbon chains are identical for DOPC and DOTAP (see Figure 2).

The peak positions of CL−DNA complexes depend on the lipid composition and the lipid-to-DNA ratio L/D. To investigate the nature of the DNA packing, we systematically varied the composition of the lipid−DNA mixtures. Let us denote the three components of the mixture: D [mg], L^0 [mg], and L^+ [mg], corresponding to the weights of DNA, neutral lipid, and cationic lipid, respectively. We introduce the following unitless parameters: the lipid-to-DNA mass ratio

$$L/D = (L^+ + L^0)/D \tag{1}$$

and the lipid-to-DNA charge ratio

$$\xi = \left(\frac{L^+}{MW(L^+)}\right)\left(\frac{MW(bp)}{2D}\right) \tag{2}$$

which is the ratio of cationic headgroups to the number of negatively charged phosphate groups along the DNA backbone. According to this definition, $\zeta = 1$ corresponds to stoichiometric charge neutrality. The mass ratio of cationic lipid to DNA in this case can be calculated using eq 2 and yields $L^+/D = 2.2$ for MW(DOTAP) = 698.6 and MW(bp) = 649 (the average molecular weight of one base pair).

We performed two series of experiments as a function of L/D, one where the lipid-to-DNA charge ratio was kept at charge neutrality $\zeta = 1$ (Figure 7) and a second one where the lipid composition was fixed at $L^+/L^0 = 1$ (Figure 8).

In the case of charge neutral complexes the only compositional degree of freedom is to vary the lipid composition L^+/L^0, i.e., increasing the amount of neutral lipid. In this case the variation can be viewed as a dilution of the one-dimensional DNA lattice through addition of a neutral lipid (Figure 7b). We will show that the DNA spacing in this case can be rigorously derived from geometric packing arguments. Figure 9 depicts a cross section of the one-dimensional DNA lattice of the lipid−DNA stack. Since the structure is invariant along the direction of the DNA strands, the ratio of lipid volume to DNA volume is equal to the ratio of the area cross sections of lipid and DNA:

$$\frac{V_L}{V_D} = \frac{\rho_D}{\rho_L}(L/D) = \frac{A_L}{A_D} \tag{3}$$

where, V_L, A_L, ρ_L and V_D, A_D, ρ_D denote the volume, area, and density of lipid and DNA, respectively. The cross-sectional area of the lipid in one lattice constant is given by $A_L = \delta_m d_{DNA}$. Hence replacing A_L in eq 4 yields the DNA−DNA packing distance

$$d_{DNA} = \frac{A_D \rho_D}{\delta_m \rho_L}(L/D) \tag{4}$$

The packing distance is linear in L/D as expected for a 1D lattice. The prefactors are known material constants. The density of a lipid membrane is on average $\rho_L = 1.07$ (g/cm^3). The DNA cross section times the DNA density is equal to the mass per unit length, which is determined by the average mass of one base pair divided by the step height between base pairs, $A_D\rho_D = MW(bp)/(6.022 \times 10^{23} d_{bp}) = 3.17 \times 10^{-14}$ g/cm, where MW(bp) = 649 denotes the average molecular weight of one base pair and $d_{bp} = 3.4$ Å. The membrane thickness is given by $\delta_m = d_{mem} - d_w$. The membrane repeat distance δ_{mem} increases with L/D due to the chain length difference of 5 Å between DOPC and DOTAP. From the measured membrane thicknesses a constant water layer thickness $d_w = 25 \pm 1.5$ Å was determined. Therefore, eq 4 predicts the DNA−DNA packing distance without any adjustable parameter. In Figure 7b the full line represents the theoretical values derived from eq 4. The agreement is remarkable and is a strong indication for the existence of a one-dimensional smectic DNA ordering. The evaluation of the width of the DNA−DNA correlation peak furthermore results in extended short-range correlations over about 8 lattice units of the 1D rod lattice.

In the lipid−DNA mixing experiment studied by optical microscopy (Figure 3) the lipid composition was kept constant $L^+/L^0 = 1$ and the lipid-to-DNA mass ratio was varied by titration of DNA to a vesicle solution. In this case the lipid/DNA charge ratio ζ is not constant but varies with the mass ratio L/D for given lipid composition L^+/L^0. For a binary (1:1) mixture of DOPC/DOTAP we obtain from eq 2 $x = 0.23$L/D and the point of charge neutrality is reached at L/D = 4.4. Figure 8b shows that the DNA correlation distance exhibits two constant regimes. One for large L/D > 4.4 with $d_{DNA} = 4\,6$ Å and another for small L/D < 4.4 with $d_{DNA} = 35$ Å. The two regimes correspond to mixtures with positive surface charge (L/D > 4.4) and negative surface charge (L/D < 4.4), respectively. The fact that the DNA packing distance is constant in both regimes can be explained by the coexistence of CL−DNA aggregates and excess DNA in the negative regime and CL−DNA aggregates and excess cationic liposomes in the positive regime. This behavior as a function of lipid dilution L/D is depicted schematically in Figure 8b. The two regimes are separated by a small region, where the data seem to fit the geometric packing model for charge neutral complexes (L/D = 4.4, dashed line in Figure 8b).

(21) Roux, D.; Safinya, C. R. *J. Phys. Fr.* **1988**, *49*, 307−318.

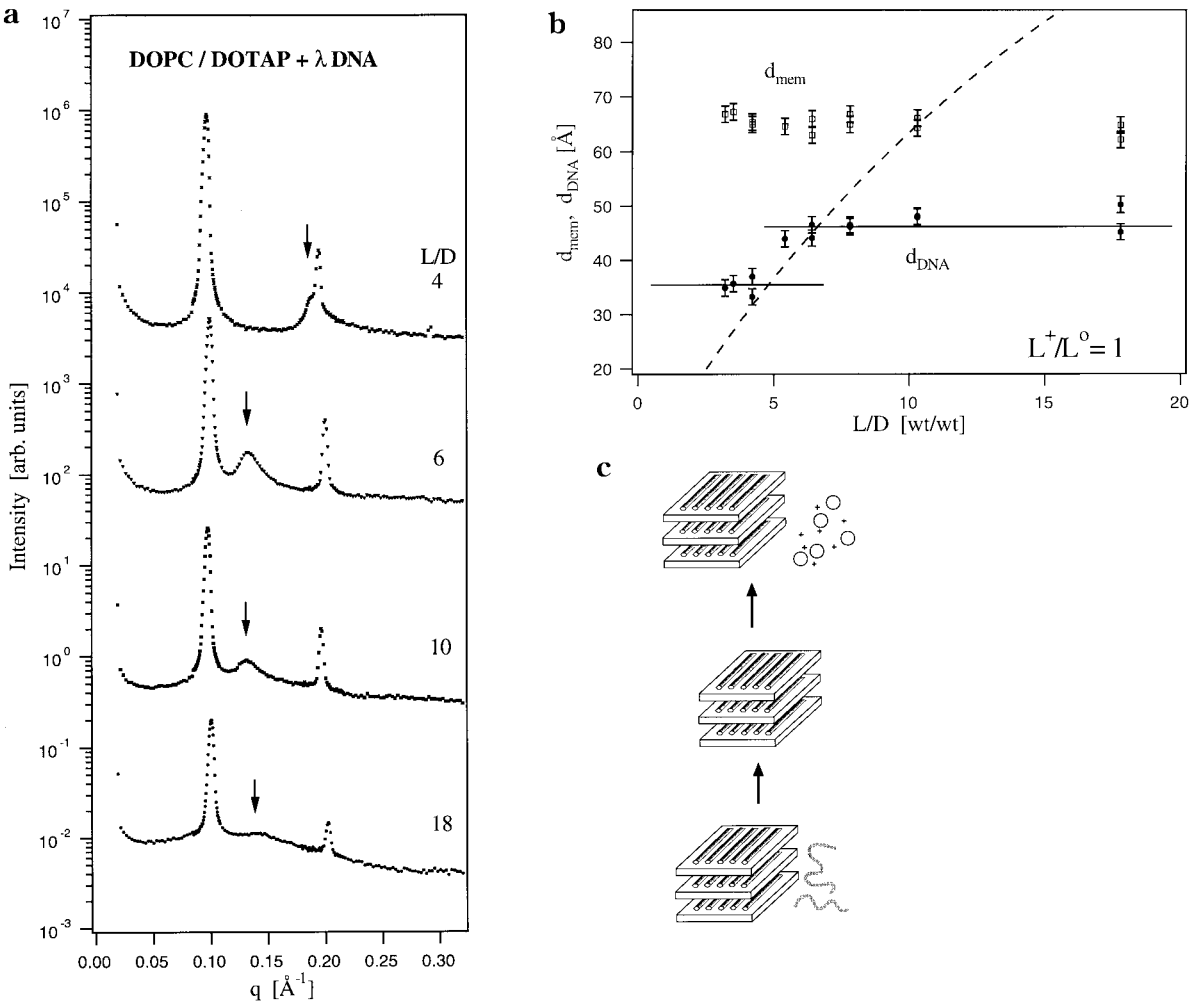

Figure 8. Synchrotron X-ray diffraction scans of DOPC/DOTAP−λ-DNA mixtures with constant lipid composition ($L^+/L^0 = 1$). The L/D mass ratio was varied corresponding to the optical L/D series shown in Figure 3. (b) Repeat distances of the scans in Figure 7a exhibiting two regimes of constant DNA−DNA spacing as a function of L/D. Aggregates with L/D < 4.4 that coexist with excess DNA show a smaller (d = 37 Å) spacing than aggregates with L/D > 4.4 that coexist with excess cationic liposomes (d = 46 Å). (c) Schematic drawing of the coexistence regimes.

Liquid Crystalline Textures. The macroscopic shape of the condensed structures is strongly dependent on the concentration and mixing conditions. We mixed a concentrated (5 mg/mL) solution of λ-DNA into an almost equal volume of a concentrated (25 mg/mL) solution of sonicated vesicles within an X-ray capillary. The lipid−DNA aggregates form immediately at the interface of the two solutions and thin sheetlike precipitates can be seen by eye (Figure 10a). We found a persistent globular morphology of connected globules at higher magnification in all our samples (Figure 10c). The texture of the globules under crossed polarizers exhibited strong birefringence of liquid crystal defects (Figure 11a), both focal conics and spherulites, known from the smectic-A-like layered structures.[22] Similar defects are also observed in the spherical and dendrite globules that form at the lower concentrations (Figure 3). What is remarkable is the retention of the globule morphology observed at lower concentrations in the concentrated samples, as shown in Figure 10c. The globular structures are often flow aligned and sometimes exhibit chiral superstructures. We observed sheetlike bands coiled into left-handed helical aggregates (Figure 10b, black arrow) and left-handed helical structures of connected globules (Figure 11b). The fact that such morphologies are found on many length scales might be indicative of a left-handed twist in the underlying liquid crystalline structure.[23]

Some long-term structural changes in concentrated samples can be observed by light microscopy. Giant excess liposomes tend to appear at the surface of the lipid−DNA condensed structures with L/D ≫ 4.4 after a couple of days, as shown in Figure 10b (white arrow). Obviously, the initial precipitation of DNA and liposomes formed a metastable structure with an excess amount of lipid. To reach the equilibrium structure, some membrane is squeezed out in the form of giant liposomes. This observation is in agreement with the fact that the position of the DNA correlation peak measured by X-ray diffraction slightly shifts during the first few days after sample preparation. Note that for any given lipid-to-DNA ratio only one equilibrium structure is formed independent of the preparation conditions. We prepared samples from lipid powder and lyophilized DNA, which after hydration, yielded an X-ray pattern identical to that of liposomal suspensions mixed with DNA solutions.

(22) Boltenhagen, P.; Lavrentotovich, O. D.; Kleman, M. *Phys. Rev. A* **1992**, *46*, 1743−1746.

(23) Kamien, R. D.; Nelson, D. R. *Phys. Rev. Lett.* **1995**, *74*, 2499−2502.

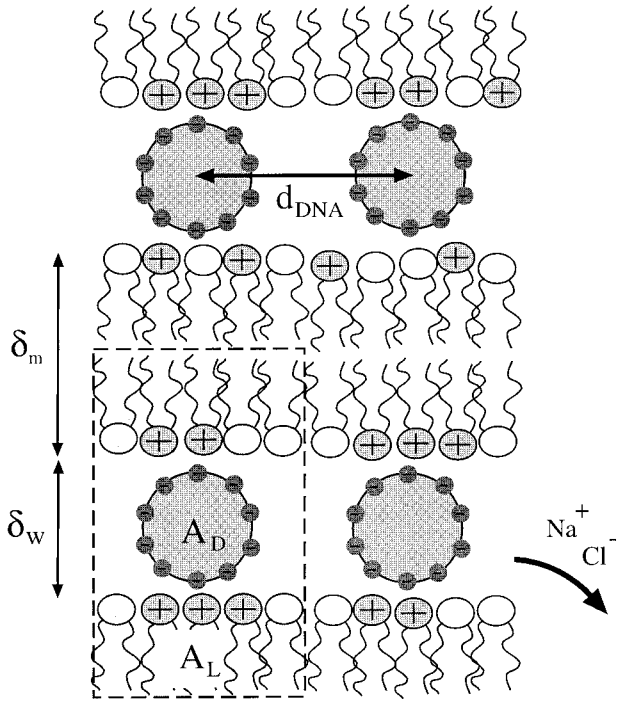

Figure 9. Schematic cut through the intercalated DNA−lipid lattice. The DNA is viewed in cross-section with the negatively charged phosphate groups on the circumference of the DNA cross-sectional area A_D. The membrane cross-section A_L and the size of the lipid molecules with respect to DNA are drawn in correct proportions, demonstrating the tight packing of charged groups.

Discussion

DNA and cationic liposomes condense into liquid crystalline aggregates, whereby the lipid-to-DNA mass ratio determines whether the complexes coexist with excess DNA or excess liposomes. We showed that the surface potential, size distribution, and internal solution structure depend on the coexistence equilibrium. Two distinct regimes were found, corresponding to two DNA packing distances with 46 Å for positive and 35 Å for negative CL−DNA complexes. A narrow transition region around the stoichiometric charge neutral ratio, $\zeta = 1$, separates the two coexistence states. A theoretical description of the thermodynamic equilibrium spacings of lamellar DNA−lipid liquid crystals in the presence of excess DNA and excess lipid was recently calculated from statistical thermodynamic models using nonlinear Poisson−Boltzmann theory.[24,25] In agreement with our experimental findings it was shown that the DNA spacing in the lamellar intercalated structure exhibits a jump around the isoelectric point. The equilibrium spacing can be understood from the fact that the complexes beyond the charge neutral ratio can take up excess material only at a cost of increasing counterion pressure. In fact, at the isoelectric point almost all the counterions are released from the complex.[26] Hence the cationic lipids act as two-dimensional "counterlipid".[24] In a thermodynamic model one has to distinguish if free lipid exchange is allowed in the vesicle−CL−DNA coexistence regime or not.[25] Exchanging lipid with the excess free bilayer the complex can increase its cationic mole fraction and hence decrease its DNA packing distance. We have found that d_{DNA} is constant above the isoelectric point (in the excess lipid regime), indicating that almost no lipid exchange takes place. The statistical thermodynamic model furthermore allows spatial inhomogeneities within the DNA condensed lipid bilayer, as shown schematically in Figure 1. The numerical Poisson−Boltzmann solution predicts that the cationic lipid concentration profile (for $L^+/L^0 < 0.7$) is enriched close to the DNA phosphate groups.[25] The phase separation is also favored from steric considerations, since the PC headgroup is about 5 Å larger than the TAP headgroup. We emphasize, however, that further and more complete investigation of the CL−DNA complex phase diagram is required in order to elucidate the interactions resulting in equilibrium complex structure and provide a meaningful test of available theories.[27]

Our model of CL−DNA complexes is based on a new multilamellar structure with intercalated one-dimensional lattices of DNA chains (i.e., a novel 2D smectic phase). This solution structure is best demonstrated along the isoelectric line, defined by the constraint of stoichiometric charge neutrality. The *variation in the DNA interaxial distance* as a function of the charged-to-neutral lipid ratio, L^+/L^0, unambiguously substantiates that (1) we directly probe the DNA behavior in multilayer assemblies and (2) the linear DNA chains confined between bilayers form a 2D smectic phase. In the isoelectric regime, the DNA interaxial distance increases from 24.5 to 57.1 Å as a function of lipid dilution and is consistent with an expanding one-dimensional lattice of DNA chains (i.e., a novel 2D smectic phase). Most convincingly, the DNA−DNA interhelical distance is predictable from a simple volume fraction model. This model requires that a repulsive interaction exists between the DNA strands, which leads to an expansion of the DNA lattice with lipid dilution, in contrast to a situation where the system would phase-separate into a DNA-rich and DNA-poor phase. In a separate study we determined the 2-dimensional compressibility modulus of the DNA lattice by line-shape analysis of the DNA correlation peak.[20] The dependence of the experimental compressibility as a function of the interrod spacing suggests that the repulsive interaction between the strands is dominated by electrostatic and hydration forces. In our model we neglect any deformation or demixing of the lipid membrane. However, the line-shape analysis gave the first evidence for the existence of out-of-plane DNA correlation.[20]

Our studies imply that the bilayer dominates the molecular ordering. It can be assumed that many complexes of DNA and bilayer-forming cationic lipid exhibit intercalated lamellar liquid crystalline structures. In fact, lamellar phases have been reported for polypeptides complexed with oppositely charged lipids or bilayer-forming surfactants.[28−31] In comparison to polypeptides or synthetic polymers, DNA is characterized by a larger persistence length (500 Å) as well as a high charge density. The common feature of these polyelectrolyte lipid composite phases is the self-assembling mechanism: the hydrophobic interaction forming the planar lipid bilayers and a strong electrostatic interaction that is responsible for the alternating layering and in-plane ordering of the cationic lipid and anionic polymer.

(24) Bruinsma, R. *J. Phys.*, in press.
(25) Harries, D.; May, S.; Gelbart, W. M.; Ben-Shaul, A. *Biophys. J.*, in press.
(26) Wagner, K.; Rädler, J. Unpublished results.
(27) Koltover, I.; Safinya, C. R. Unpublished results.
(28) de Kruijff, B.; Rietveld, A.; Telders, N.; Vaandrager, B. *Biochim. Biophys. Acta* **1985**, *820*, 295−304.
(29) Antonietti, M.; Conrad, J.; Thünemann, A. *Macromolecules* **1994**, *27*, 6007−6011.
(30) Ponomarenko, E. A.; Waddon, A. J.; Bakeev, K. N.; Tirrell, D. A.; MacKnight, W. J. *Macromolecules* **1996**, *29*, 4340−4345.
(31) Zschörnig, O.; Arnold, K.; Richter, W.; Ohki, S. *Chem. Phys. Lipids* **1992**, *63*, 15−22.

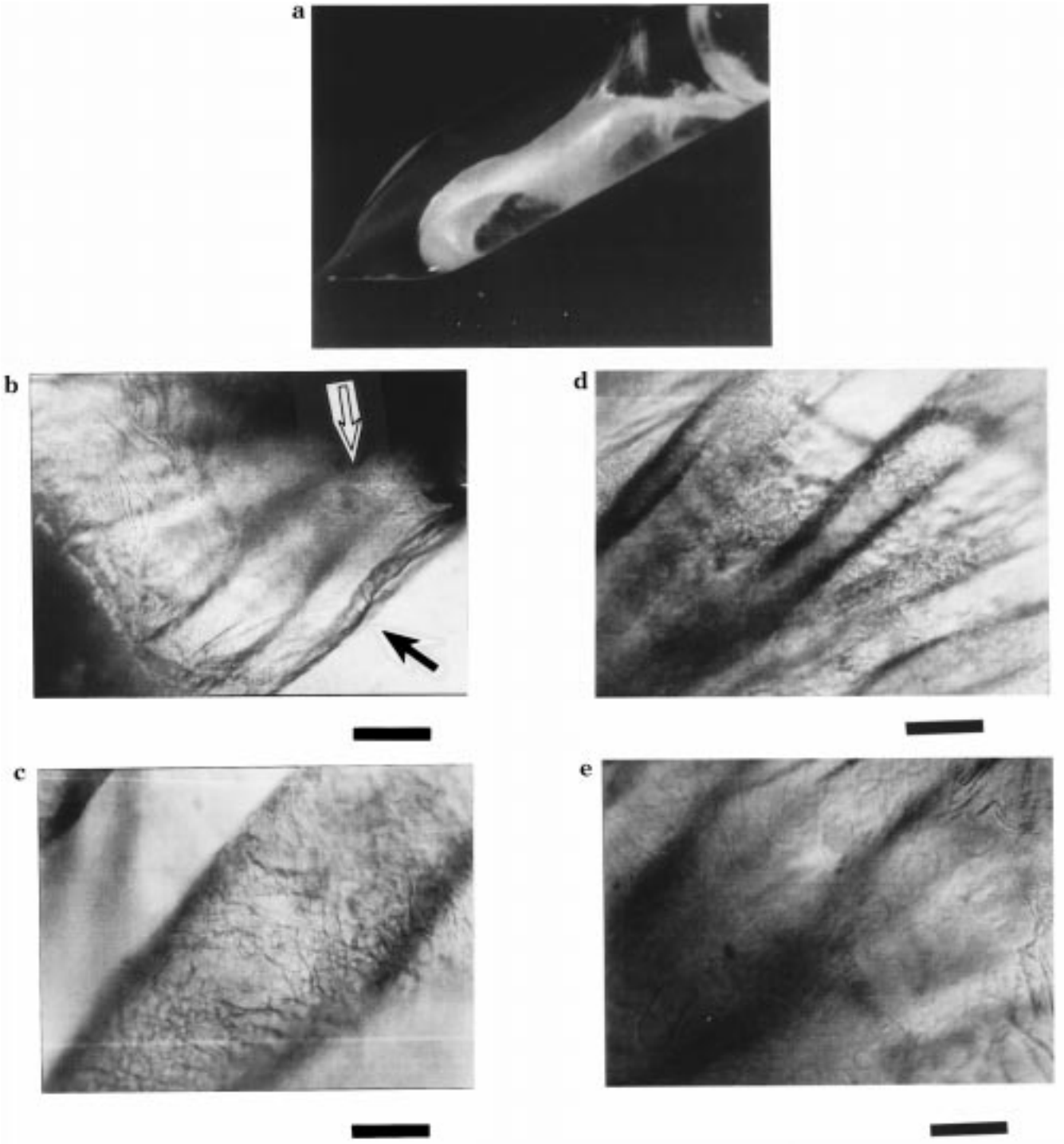

Figure 10. (a) Photograph of a concentrated sample of a sheet-like CL−DNA precipitate sealed in a 2 mm X-ray capillary. (b) Bright field microscopy images of a CL−DNA complex with L/D = 10. Giant liposomes can be seen to extrude out of the complexes (white arrow). In addition, macroscopic helical aggregates are observed (black arrow) (bar = 200 μm). (c) Higher magnification of the sample shown in (b) reveals the globular morphology of the CL−DNA complexes (bar = 50 μm). (d) Flow-aligned bands of complexes, which show giant liposomes (e) on top of the liquid crystalline globules. (bar = 200 μm).

Recently, atomic force microscopy was applied to image DNA adsorbed to supported cationic lipid bilayers.[32,33] Fingerprint textures were found which showed remarkable constant DNA−DNA interhelical spacings. Hence, DNA adsorbed to a single cationic lipid layer forms a two-dimensional smectic phase as well as the three-dimensional intercalated complexes. Surprisingly, the interhelical spacing differs by a factor of 2 from the spacing predicted by eq 4 for the three-dimensional complexes. However, if it is taken into account that only one side of the bilayer is in contact with the DNA, the interhelical distance of 46 Å measured on pure DPDAP and DSDAP bilayers is in good agreement with our data. In other words, the adsorbed DNA monolayer forms an approximately charge neutral complex with the cationic lipid monolayer facing the solution.

(32) Mou, J.; Czajkowsky, D. M.; Zhang, Y.; Shao, Z. *FEBS Lett.* **1995**, *371*, 279−282.
(33) Fang, Y.; Yang, J. *J. Phys. Chem. B* **1997**, *101*, 441−449.

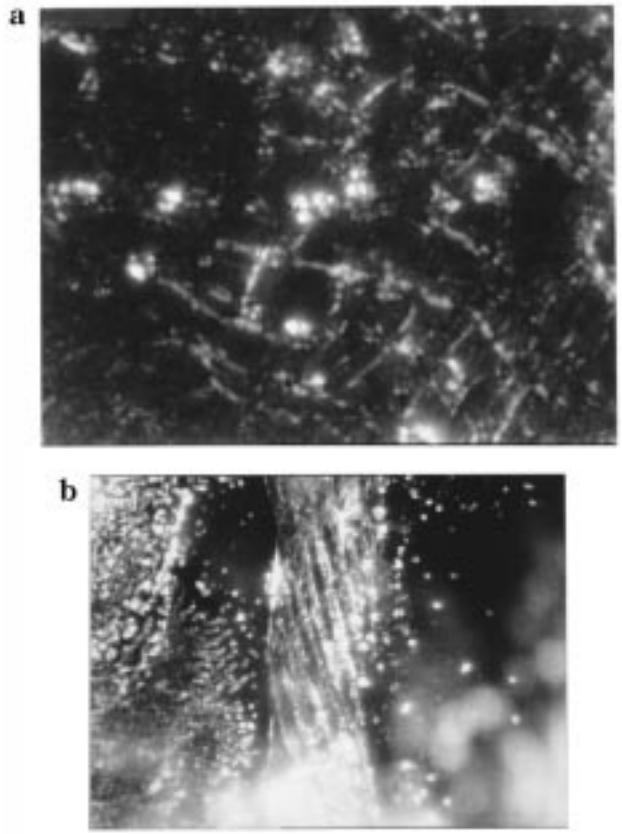

Figure 11. (a) Micrographs under crossed polarizers showing liquid crystalline-like defects (spherulites) typical for smectic A liquid crystals (bar = 25 μm). (b) Helical superstructure of globules possibly induced by the chirality of DNA (bar = 100 μm).

Our optical investigations demonstrated that DNA−lipid complexes can be understood as colloidal particles. For medical applications the stability as well as the shape and size distribution of the complexes is important. Small, well-defined, monodisperse aggregates are preferred.[34] Our data allows one to predict the DNA packing density and the surface charge of complexes. Their surface charge and size can be derived from the lipid-to-DNA ratio. Therefore, the understanding of molecular packing may be valuable for the development of new synthetic gene carriers. In particular the rational design of multicomponent higher-order complexes will depend on a better understanding of the self-assembling forces and principles of self-organization. One example is the design of virus-like synthetic complexes coated with endosomolytic peptides[35,36] or specific ligands to achieve targeted delivery.[37,38] Equally important will be to gain insight into the changes going on inside the complexes during the path of transfection.[14,39] The fact that the molecular structure and interfacial properties of CL−DNA depend on the coexistence condition with DNA or liposomes suggests that they will also strongly depend on other external conditions.

Acknowledgment. We acknowledge useful discussions with P. Pincus, R. Bruinsma, T. Lubensky, W. Gelbart, and N. Dan. The work was partially supported by NSF grant DMR-9624091, the Petroleum Research Fund (No. 31352-AC7), and Los Alamos CULAR grant No. STB/UC:95-146. J.R. gratefully acknowledges support by DFG scholarship Ra 655/1-1. The Materials Research Laboratory at Santa Barbara is supported by the NSF under grant DMR-9123048. The synchrotron experiments were carried out at Stanford (SSRL) supported by the U.S. DOE.

LA980360O

(34) Hofland, H. E. J.; Shephard, L.; Sullivan, S. M. *Proc. Natl. Acad. Sci. U.S.A.* **1996**, *93*, 7305−7309.
(35) Wagner, E.; Plank, C.; Zatloukal, K.; Cotten, M.; Birnstiel, M. L. *Proc. Natl. Acad. Sci. U.S.A.* **1992**, *89*, 7934−7938.
(36) Moradpour, D.; Schauer, J. I.; Zurawski, V. R.; Wands, J. R.; Boutin, R. H. *Biochem. Biophys. Res. Commun.* **1996**, *221*, 82−88.
(37) Remy, J.-S.; Kichler, A.; Mordvinov, V.; Schuber, F.; Behr, J.-P. *Proc. Natl. Acad. Sci. U.S.A.* **1995**, *92*, 1744−1748.
(38) Lee, R. J.; Huang, L. *J. Biol. Chem.* **1996**, *271*, 8481−8487.
(39) Zelphati, O.; Szoka, F. C. J. *Proc. Natl. Acad. Sci. U.S.A.* **1996**, *93*, 11493−11498.